Structure Functions

W.J. Stirling

Departments of Mathematical Sciences and Physics
University of Durham, Durham DH13LE, UK

Abstract

We review recent theoretical progress in the study of deep inelastic structure functions. Three topics are considered in detail: global parton distribution analyses, small-x physics, and structure functions at low Q^2.

Résumé

Nous décrivons les progres théoretiques récents dans l'étude des fonctions de structure inélastique profondes. Trois sujets sont étudiés en detail: analyses globales des distributions de partons, physique de petit x, et fonctions de structure à petit Q^2.

1. Introduction

Since the Eilat Deep Inelastic Scattering Conference in 1994 there have been several important advances in our knowledge of the parton structure of hadrons. Further measurements of the structure function $F_2^{ep}(x,Q^2)$ at HERA have shed more light on the small-x behaviour of the quark and gluon distributions and brought into sharper focus the difference betwen the various theoretical approaches: 'BFKL', 'GLAP' 'dynamical partons, 'double asymptotic scaling', and so on. New high-precision measurements at hadron colliders, in particular of the Drell-Yan asymmetry and the W charged lepton asymmetry, when combined with fixed-target structure function measurements now determine very precisely the shape of the u-quark and d-quark distributions at medium-high x. Finally, the measurements (in particular by the E665 collaboration) of structure functions at very low x and Q^2 allow the perturbative–non-perturbative transition region to be explored quantitatively.

In this brief review I will discuss several of these advances. In the following section I describe how the new experimental information is interpreted in terms of global analyses of parton distributions, using the framework of leading-twist, next-to-leading order perturbative evolution. In Section 3 some of the recent theoretical developments in small-x physics are discussed, and in Section 4 the impact of the new structure function data at low Q^2 is assessed.

2. Global parton distribution analyses

There are currently three theoretical collaborations producing sets of parton distributions which are widely used in high-energy collider phenomenology: CTEQ (Collaboration for Theoretical and Experimental Studies in Quantum Chromodynamics), MRS (Martin–Roberts–Stirling) and GRV (Glück–Reya–Vogt). The first two of these use the concept of 'global fits' to determine each parton distribution as accurately as possible from high-precision data on deep inelastic structure functions and other hard scattering processes. The GRV analysis is in the context of the 'dynamical parton model' [1] in which the partons evolve from valence-like distributions at a low Q^2 scale. These starting distributions are tuned to fit the data at higher Q^2.

All of the above distributions have evolved over the years as the quality of the data has improved. At the present time they all agree very well with a wide range of experimental measurements, and as a consequence the parton distributions are broadly similar. In fact since all the collaborations use the framework of next-to-leading order (NLO) fits in the $\overline{MS}$ factorization scheme, direct comparisons are possible (see below). More detailed descriptions of the CTEQ and GRV distributions can be found in the contributions of Owens [2] and Vogt [3]. Here I will focus mainly on the updates which have been performed in the last year, and on the similarities and differences between the various sets.

Process/ Experiment	**Leading order subprocess**
DIS ($\mu N \to \mu X$) BCDMS, NMC $F_2^{\mu p}, F_2^{\mu n}$	$\gamma^* q \to q$
DIS ($\nu N \to \mu X$) CCFR (CDHSW) $F_2^{\nu N}, xF_3^{\nu N}$	$W^* q \to q'$
$\mu N \to c\bar{c}X$ F_2^c, EMC	$\gamma^* c \to c$
$\nu N \to \mu^+\mu^- X$ CCFR	$W^* s \to c \hookrightarrow \mu^+$
DIS (HERA) F_2^{ep} (H1,ZEUS)	$\gamma^* q \to q$
$pp \to \gamma X$ WA70, UA6	$qg \to \gamma q$
$pN \to \mu^+\mu^- X$ E605	$q\bar{q} \to \gamma^*$
$pp, pn \to \mu^+\mu^- X$ NA51	$u\bar{u}, d\bar{d} \to \gamma^*$ $u\bar{d}, d\bar{u} \to \gamma^*$
$p\bar{p} \to WX(ZX)$ UA2, CDF, D0	$ud \to W$
$\to W^{\pm}$ asym CDF	$ud \to W$

2.1. Recent updates

The main changes to the global parton distributions in the last year have resulted from the improved precision of the HERA structure function (F_2) data at small x.

- The MRS(A) distributions [4] first presented at the Eilat DIS Conference in 1994 were extended to lower Q^2 in Ref. [5] (see also Section 4), and recently replaced by the MRS(A′) distributions in Ref. [6]. At the same time, a new set of distributions, MRS(G), was introduced to investigate the possibility that the quark and gluon starting distributions have a rather different $x \to 0$ behaviour. This will be described further in Section 2.4. The data sets which are used in the latest MRS fits are shown in the accompanying table, together with the leading-order parton subprocesses which are probed.
- The CTEQ2 distributions of late 1993 [7] were extended in 1994 to the CTEQ3 sets [8]. Three versions of the latter are provided: $\overline{MS}$ and DIS factorization schemes (CTEQ3M,CTEQ3D) at next-to-leading order, and a leading-order fit (CTEQ3L).
- The 1992 GRV distributions [9] were updated in 1994 [10] to give a slightly better fit to the small-x HERA structure function data. The philosophy remains the same: valence-like quark and gluon distributions (i.e. $xf(x,\mu_0^2) \to 0$ as $x \to 0$, $f = q, g$) are GLAP-evolved [11] from a low starting scale μ_0 in both leading (GRV(LO)) and next-to-leading order (GRV(HO)) perturbative QCD. The starting distributions are carefully tuned to reproduce the large-x structure function data: in practice this involves fitting the valence-quark distributions to the MRS(A) distributions at $Q^2 = 4\ GeV^2$. The essential difference between the GRV92 and GRV94 versions is that the starting scale is increased from $\mu_0^2 = 0.3\ GeV^2$ to $\mu_0^2 = 0.34\ GeV^2$ in the latter. This has the effect of decreasing the 'evolution length', giving a less steeply rising structure function in the HERA kinematic regime, in better agreement with the most recent data. Another important feature of the GRV distributions is that the charm and bottom quarks are both treated as 'heavy' quarks, and not included in the parton content of the proton. The charm contribution to the structure function is then obtained by folding the appropriate hard scattering subprocess with the gluon distribution: schematically,

$$F_2^c = \hat{\sigma}(\gamma^* g \to c\bar{c}) \otimes g. \qquad (1)$$

Note that this represents a different philosophy from the MRS and CTEQ approaches, where both c and b distributions are evolved as massless partons above their excitation thresholds and $F_2^c = \frac{8}{9} xc$. It will be interesting to see which of these two approaches gives a better description of the charm component of F_2 at HERA, when this is eventually measured. The

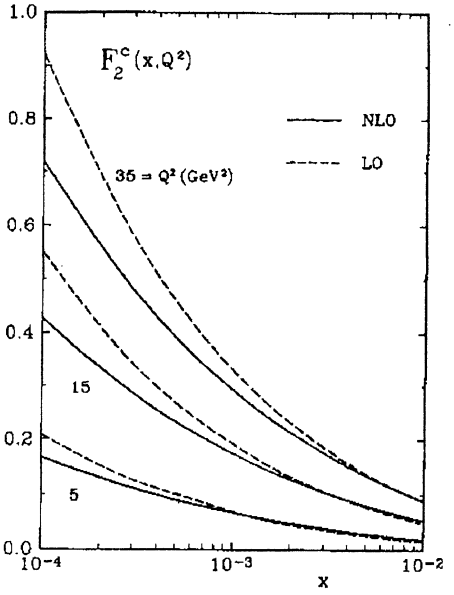

Figure 1. *GRV prediction for the charm contribution to F_2^{ep} at HERA, from Ref. [10].*

GRV prediction for $F_2^c(x, Q^2)$ is shown in figure 1. Note that the next-to-leading order correction is not negligible at very small x.

2.2. A comparison between the MRS and CTEQ sets

Since the MRS and CTEQ global analyses are similar in spirit, it is instructive to compare the resulting parton distributions in some detail. The first point to note is that since the fitted data sets in the most recent versions are almost identical, so are the resulting parton distributions. Over most of the x range the differences in the individual distributions (at $Q^2 \sim Q_0^2$) are typically of the order of a few per cent. Both groups now rely heavily on the NA51 Drell-Yan asymmetry [12] and the CDF charged lepton asymmetry [13] data to constrain the $\bar{d}/\bar{u}$ and d/u distributions respectively. As an illustration, figure 2 (from Ref. [8]) shows the quality of the fits to the CDF lepton asymmetry data in the recent MRS and CTEQ analyses.

In contrast to earlier sets, the procedure for parametrising the starting distributions (at $Q_0^2 = 4\ GeV^2$) is also very similar. In each case the generic form

$$xf_i(x, Q^2) = A_i x^{-\lambda_i}(1 + b_i\sqrt{x} + c_i x)(1 - x)^{a_i} \qquad (2)$$

is used, although for some (particularly gluon and sea quark) distributions certain ill-determined parameters are set to zero. In all there are 18 (15) shape parameters in the most recent MRS [4, 6] (CTEQ [8]) sets respectively. The smaller number of CTEQ parameters is in part due to the omission from the fit of some low-x fixed target data (see below).

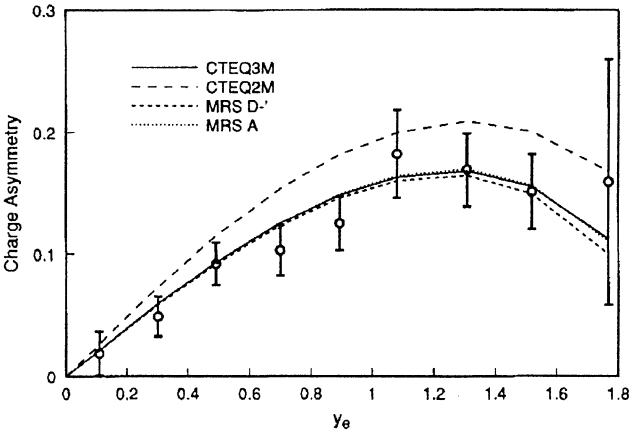

Figure 2. *CDF charge lepton asymmetry data [13] with recent parton distribution fits, from Ref. [8].*

A slightly different procedure is also used for normalising the various deep inelastic structure function data sets. In the CTEQ analysis the normalisation of each data set is allowed to vary independently within the quoted experimental uncertainty. In contrast, MRS use the SLAC/NMC data [14, 15] as the baseline, and adjust the normalisation of the other data sets to give the optimum fit. In the medium-x region this results in a systematic difference between the dominant (u,d) quarks in the two sets:

$$q_{CTEQ} \simeq 1.02\, q_{MRS}\ . \qquad (3)$$

It is interesting that this difference can be observed in, for example, the predicted top quark production cross section at the Tevatron, which samples the product of (u,d) quark distributions at $x \sim 0.25$, see figure 3.

The most significant difference, however, arises from the omission in the CTEQ global fit of the small-x (< 0.09) fixed target CCFR $F_2^{\nu N}, F_3^{\nu N}$ [16] and NMC $F_2^{\mu n, \mu p}$ [15] data. It has been known for some time (see for example Ref. [17]) that it is difficult to reconcile these two data sets with the additional observation [18] that the strange quark is suppressed by about 50% compared to the other light quarks in the sea, i.e. $s \approx (\bar{u} + \bar{d})/4$. Both data sets *are* included in the MRS analysis, and the resulting best fit tends to favour the slightly more precise NMC data. Without the constraints from data, the CTEQ u and d quark distributions undershoot the corresponding MRS distributions in this medium-small x region, see figure 4.

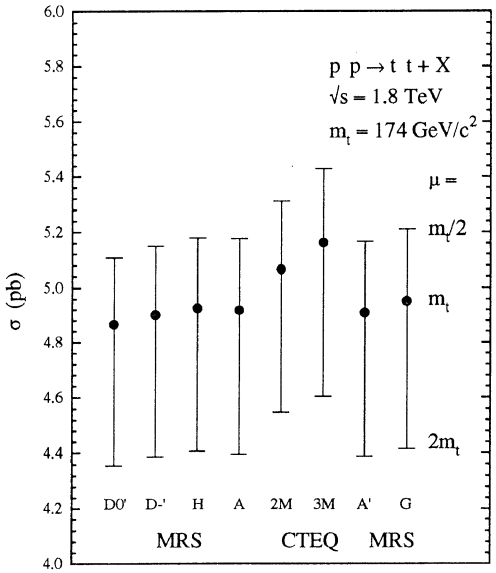

Figure 3. *Parton distribution and (factorisation/renormalisation) scale dependence of the predictions for $\sigma(t\bar{t})$ at the Tevatron.*

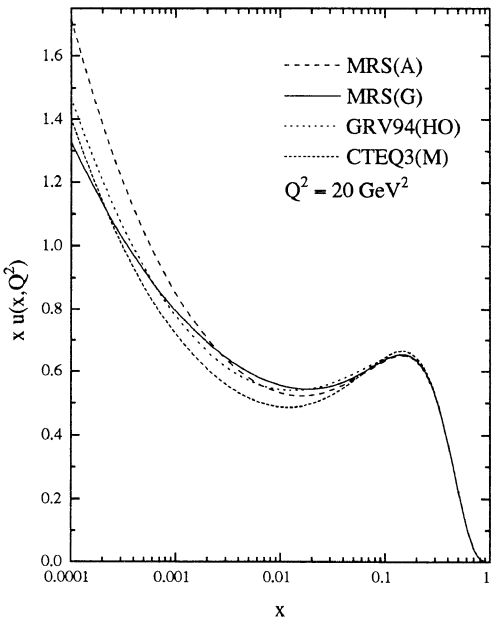

Figure 4. *u-quark distributions from several recent parametrisations, at $Q^2 = 20\ GeV^2$.*

2.3. Other global analyses

Mention should be made of several other 'global' parton analyses. Capella et al. [19] have presented a unified Regge-based treatment of the $\sigma^{\gamma p}$ photoproduction cross section and the low-Q^2 structure functions, which is matched to NLO GLAP evolution at high Q^2. There is a small number of fitted parameters. In this approach the small-x behaviour of the structure function is controlled by a Q^2-dependent Regge intercept:

$$F_2 \sim x^{-\Delta(Q^2)}, \quad \Delta(Q^2) = \Delta_0 \left(1 + \frac{2Q^2}{Q^2 + d}\right), \qquad (4)$$

where the parameters are such that $0.08 \leq \Delta \leq 0.24$ for $0 \leq Q^2 \leq \infty$. This gives a reasonable description of the small x fixed-target and HERA structure function data [19].

Bourrely and Soffer [20] have presented a unified (LO) treatment of both polarised and unpolarised parton distributions, based on Fermi-Dirac and Bose-Einstein distributions for quarks and gluons respectively. Again, there is a relatively small number of free parameters in the model, and the agreement with the data is reasonable, especially for the relative sizes of the u, d and $\bar{u}$, $\bar{d}$ distributions.

Finally, both the H1 and ZEUS collaborations have preformed their own NLO GLAP-based fits to the HERA F_2 data, supplemented by fixed-target F_2 data at larger x [21, 22].

2.4. The gluon distribution

The gluon is traditionally the least well-determined of all the parton distributions, contributing only at next-to-leading order in deep inelastic structure functions. The best determination at medium and large x comes from large p_T direct photon production in hadron-hadron collisions, and all the global parton analyses incorporate such data in the fits (see below). Other processes such as (i) inelastic lepto- and photoproduction of J/ψ, and (ii) dijet production in photon-proton collisions at HERA and proton-antiproton collisions at the Tevatron provide information which is complementary but not yet competitive in precision.

The new HERA measurements of F_2 provide for the first time a reliable estimate of the gluon at small x via the evolution equations [11] for the Q^2 dependence of F_2 which, for $x \lesssim 0.01$, can be approximated by

$$\frac{\partial F_2(x,Q^2)}{\partial \log Q^2} \simeq \frac{\alpha_s(Q^2)}{\pi} \sum_q e_q^2$$

$$\times \int_x^1 \frac{dy}{y} \left(\frac{x}{y}\right) P_{qg}\left(\frac{x}{y}\right) yg(y, Q^2). \tag{5}$$

In fact the most recent HERA data show that at small x F_2 is rising slightly faster with Q^2 than is predicted by sets such as MRS(A) (and its successor MRS(A')) in which the small-x behaviour of the sea quarks and gluons are tied together, in particular by imposing $\lambda_{\bar{q}} = \lambda_g$ in the notation of Eq. (2). The MRS group has therefore performed a new global fit (denoted by MRS(G)) in which $\lambda_{\bar{q}}$ and λ_g are allowed to vary independently. The observed more rapid increase of F_2 with increasing Q^2 is accommodated by having $\lambda_{\bar{q}} = 0.067 < \lambda_g = 0.301$, which corresponds to a *flatter* sea-quark distribution and a *steeper* gluon distribution. The numerical values of the other parameters in the fit are listed in Ref. [6]. The situation is summarised in figure 5, which shows the theoretical predictions and experimental measurements of the structure function F_2 at a 'typical' small-x value, $x = 0.0004$. The MRS(A') and MRS(G) curves are labelled with their gluon and singlet quark effective λ values at this x and the starting value $Q^2 = 4$ GeV^2.

It is important to note that the resulting MRS(G) 'singular' gluon and 'flat' sea quark distributions do not have a ready explanation in terms of either perturbative or non-perturbative QCD. On the one hand GLAP evolution from a low scale, such as performed by GRV [10], develops both a steep gluon *and* a steep sea quark distribution at small x. The former is evident in the data, the latter is not. Again figure 5 summarizes the situation. The GRV(94) curve has a similar slope to MRS(G) (both gluons are steep) but overestimates the data (the GRV quarks are steeper than the MRS(G) quarks). On the other hand it might be argued that the leading $\log(1/x)$ resummation, encapsulated in the BFKL equation (see below), is more appropriate at small x. A singular (unintegrated) gluon is obtained, as required by the data, but again the steepness is fed directly into the sea quark distribution and hence into F_2. Another possible explanation is that the application of next-to-leading order, leading-twist QCD in the HERA small-x regime is simply too naive, see Section 3.

Although the quark distributions of the MRS(A') and MRS(G) sets are very similar, there is a sizable difference in the gluon distributions, particularly at small x. This difference is illustrated in figure 6, which also indicates the x range of the various experimental constraints on the gluon. Comparing the G and A' gluons, we see that (i) the new HERA measurements of $\partial F_2/\partial \log Q^2$ lead to an enhancement of the gluon for $x \lesssim 0.01$, (ii) the fixed-target prompt photon data require the gluon to be unchanged for $0.35 \lesssim x \lesssim 0.55$,

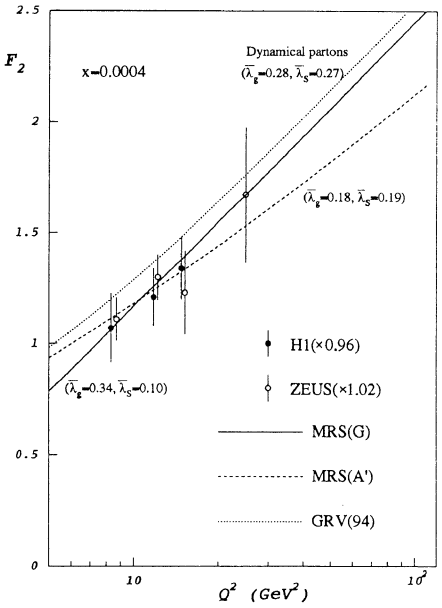

Figure 5. *The description of the H1 [21] and ZEUS [22] measurements of $F_2(x, Q^2)$ near $x = 0.0004$ compared with the MRS(A') and MRS(G) partons of Ref. [6] (dashed and solid curves respectively), and the GRV(94) partons of Ref. [10] (dotted curve).*

see figure 7 below, and (iii) as a consequence the G gluon is reduced in the intermediate interval $0.02 \lesssim x \lesssim 0.2$.

As mentioned above, prompt photon production in hadron-hadron collisions serves as a strong constraint on the gluon since it contributes directly at leading order. The CTEQ, GRV and MRS global analyses have all used fixed-target and collider data (see figure 6) to pin down the gluon at medium and large x [8, 10, 6]. In general, it is possible to obtain a satisfactory next-to-leading order QCD description of the prompt photon data. An example of the quality of the description is shown in figure 7, from Ref. [6], see also Refs. [8, 23, 24, 25].

There may however be a slight problem in that the p_T^γ distributions observed by the CDF [26] and UA2 [27] collaborations are a little steeper than is predicted. This could be due to either residual scale ambiguities in the NLO QCD calculation [25], ambiguities in the photonic fragmentation contributions [24], the presence of intrinsic k_T arising from non-perturbative or 'soft' perturbative effects [23], or (as seems most likely) a combination of all of these. Notice that the steeper MRS(G) gluon only gives a marginal improvement in the quality of the fit.

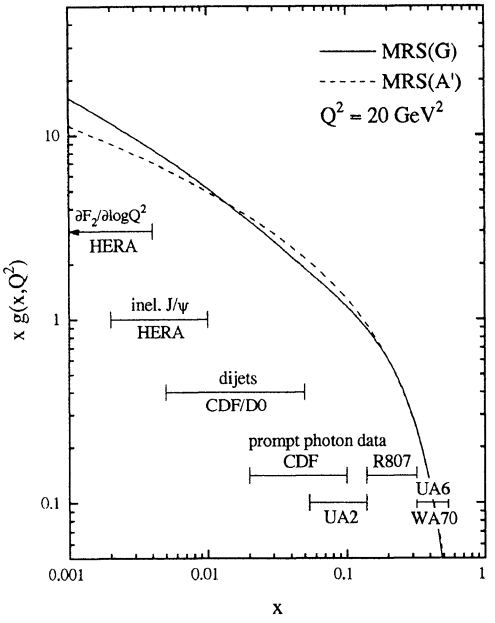

Figure 6. *The MRS(A') and MRS(G) gluon distributions at $Q^2 = 20$ GeV^2 [6]. Also shown are the x intervals in which the gluon is constrained by the various sets of data.*

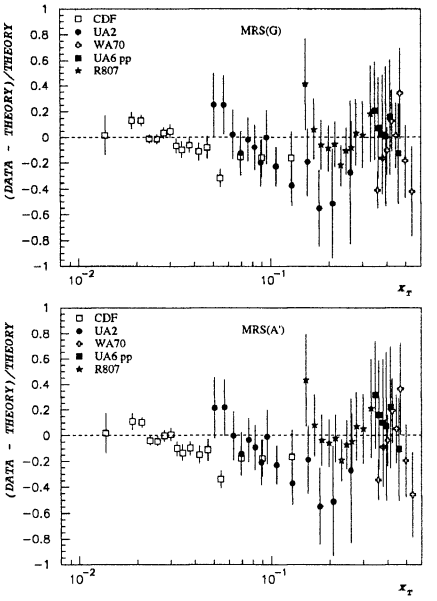

Figure 7. *Description of prompt photon data by the MRS(A') and MRS(G) parton distributions from Ref. [6].*

2.5. Determination of the strong coupling in fits to deep inelastic data

Analysis of the Q^2 dependence of deep inelastic scattering structure function data in the framework of next-to-leading order GLAP evolution provides one of the most accurate ways to determine the strong coupling α_s. The scaling violations observed in recent high precision muon and neutrino deep inelastic data yield values of $\alpha_s(M_Z^2) = 0.113 \pm 0.005$ [28] and 0.111 ± 0.006 [16] respectively. Global parton distributions analyses yield similar values; the MRS(A) fit gives $\alpha_s = 0.113 \pm 0.005$ for example [4]. An independent structure function measurement based on the Gross–Llewellyn Smith sum rule

$$I_{GLS}(Q^2) = \frac{1}{2}\int_0^1 dx \left(F_3^{\nu p}(x,Q^2) + F_3^{\bar{\nu} p}(x,Q^2)\right) = 3\left[1 - \frac{\alpha_s(Q^2)}{\pi} + \mathcal{O}(\alpha_s^2)\right] \quad (6)$$

by the CCFR collaboration [29] gives

$$\alpha_s(M_Z^2) = 0.108^{+0.003}_{-0.005}(\text{stat.}) \pm 0.004(\text{sys.}_1)^{+0.004}_{-0.006}(\text{sys.}_2), \quad (7)$$

where the second systematic error comes from an estimate of the higher-twist ($\sim 1/Q^2$) corrections to the perturbative QCD prediction in Eq. (6). This is evidently in good agreement with the value obtained from scaling violations.

However, there are other independent determinations which lie outside this range; for example the most recent value of α_s determined from the global Standard Model fit to LEP data, which is dominated by the total hadronic decay width of the Z^0, is [30]

$$\alpha_s(M_Z^2) = 0.125 \pm 0.004(\text{stat.}) \pm 0.002(\text{sys.}), \quad (8)$$

signficantly larger than the DIS value, and with comparable precision.

The determination of α_s from jet rates in deep inelastic scattering at HERA [21, 22] requires, as input to the analysis, parton distributions which have their own particular value of α_s. An obvious question of consistency arises: does the *output* α_s depend on the *input* value of α_s? To investigate this requires a series of parton distribution sets extracted from global fits for various fixed values of α_s.

In an analysis several years ago [31], the MRS group did provide 4 parton sets which covered a limited range of α_s. The CTEQ collaboration [8] have recently

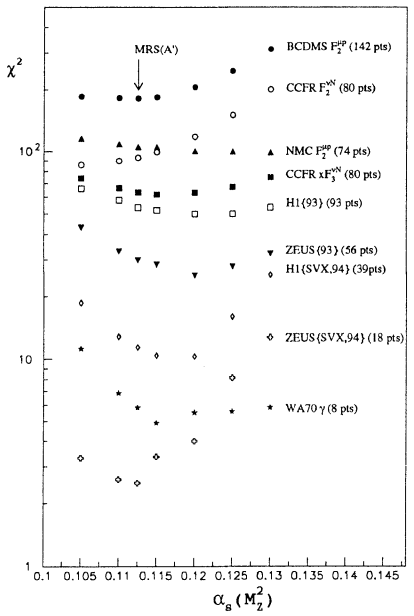

Figure 8. *Variation of χ^2 with α_s in the global fits of Ref. [33].*

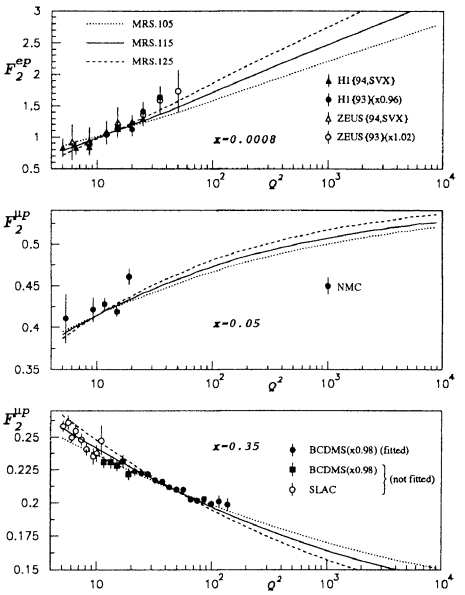

Figure 9. *Scaling violations of F_2^{lp} at three difference values of x, from Ref. [33].*

presented an additional parton set with a high α_s. At this meeting two new theoretical analyses have been reported. Vogt has provided a series of 5 GRV-type distributions with $\Lambda^{(4)}_{\overline{MS}} = 100 + 50n$ MeV, $n = 1, ..., 5$ [32]. However this is not a global analysis, and so cannot accommodate the variation of partons, particularly at larger x, which attempt to compensate for the shift of α_s from its optimum value. The MRS group has repeated the global analysis of Refs. [4, 6] for the (fixed) values of $\alpha_s(M_Z) = 0.100 + 0.005n$, $n = 1, ..., 6$ [33]. This study allows the deep inelastic data that particularly constrain α_s to be identified, and also provides a quantitative estimate of the uncertainty associated with the parton distributions $f_i(x, Q^2)$ in different regions of x and Q^2.

The χ^2 values for various subsets of deep inelastic data obtained in the six new MRS global fits are shown in figure 8. Cross section and asymmetry data for Drell-Yan and W hadroproduction are included in the analysis, but their contributions to χ^2, which are essentially independent of α_s, are not shown. Due to the logarithmic scale that has been used for χ^2 it is easy to be misled by figure 8 about the relative importance of various data sets in the determination of α_s. The χ^2 profiles at the top of the plot have a more significant impact than those which lie lower down.

Insight into the effect of varying α_s (and the related ambiguities) can be obtained from figure 9. This shows the available data for $F_2^{ep} = F_2^{\mu p}$ at three particular x values: $x = 0.0008$ in the HERA range, $x = 0.05$ which is relevant for W production at Fermilab and $x = 0.35$ representative of the large x BCDMS precision data [34] that provide the tightest constraints on α_s. The curves are obtained from the three parton sets that have $\alpha_s = 0.105, 0.115$ and 0.125. As expected, the scaling violation is greatest for the partons with the largest value of α_s. Also, as may perhaps be anticipated, the curves cross in the region of the data, which lie in different intervals of Q^2 for the different values of x. Away from the (x, Q^2) domain of the data the predictions show a considerable spread. For example for $x = 0.0008$ and $Q^2 \sim 10^3$ GeV^2 we see a sizeable variation in the prediction for F_2^{ep}. The ambiguity in the small x domain is actually greater than that shown, since the quark sea and the gluon have been constrained to have the same small x behaviour, i.e. $\lambda_{\bar{q}} = \lambda_g$ in the notation of Eq. (2). In fact the sensitivity of the predictions at small x to the interplay between the form of the gluon and the value of α_s demonstrates the importance of a global analysis which includes the crucial large x constraints on α_s. The χ^2 profiles shown in figure 8 that are obtained from the HERA data

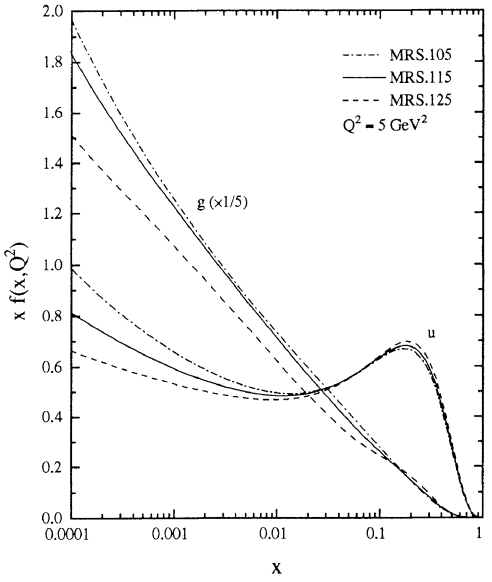

Figure 10. *The xg and xu parton distributions for the MRS sets with $\alpha_s = 0.105, 0.115, 0.125$, at $Q^2 = 20$ GeV^2 [33].*

overconstrain α_s since they are based on fits which set $\lambda_{\bar{q}} = \lambda_g$. In the global analysis this has a negligible effect on the partons, except at small x, where for Q^2 values away from the HERA data there will be more variation than implied by the spread in the curves in figure 9. The lower plot in figure 9 shows a typical set of the high precision BCDMS data [34]. In the large x domain these data place tight constraints on α_s, free from the ambiguity associated with the gluon.

The gluon and up quark distributions from three of the MRS parton sets with different α_s values are shown in figure 10 for $Q^2 = 5$ GeV^2. The systematics displayed in this plots may be anticipated from figure 9.

3. Structure functions at small x

The form of the structure functions and parton distributions in the small-x region is of considerable theoretical interest and has consequently attracted much attention. In this section we review some of the recent developments.

3.1. Higher-order corrections to the GLAP equation

The splitting functions which appear on the right-hand side of the GLAP equation have a perturbative expansion in powers of α_s. Taking a 'pure glue' theory for illustration, we have

$$t\frac{\partial}{\partial t}g(x,t) = \int_x^1 \frac{dy}{y} P\Big(\frac{x}{y}, \alpha_s(t)\Big) g(y,t), \qquad (9)$$

where $t \equiv Q^2$, and

$$P(z,\alpha_s) = P^{(1)}(z)\frac{\alpha_s}{2\pi} + P^{(2)}(z)\left(\frac{\alpha_s}{2\pi}\right)^2 + \ldots. \qquad (10)$$

The function $P^{(1)}$ is the familiar leading-order splitting function ($\equiv P^{gg}$) [11], $P^{(2)}$ gives the next-to-leading order correction, and so on. In the global parton analyses described in Section 2, only the first two terms in the perturbation theory are retained. It can be shown that away from $x = 0$ and $x = 1$ this is a good approximation, in that the NLO correction to the LO evolution is quite small.

However care must be taken at small x, where large logarithms of $L_x \equiv \ln(1/x)$ can appear in the higher-order contributions to the splitting functions and spoil the convergence. In general one can show that

$$\begin{aligned} xP^{(n)}(x) &= A_{n,n-1}L_x^{n-1} + A_{n,n-2}L_x^{n-2} + \ldots \\ &\quad + A_{n,0} + x\overline{P}^{(n)}(x), \end{aligned} \qquad (11)$$

where $\overline{P}^{(n)}$ is finite in the limit $x \to 0$. The full splitting function is then

$$xP(x,\alpha_s) = \sum_{n=1}^{\infty}\left(\frac{\alpha_s}{2\pi}\right)^n \left[\sum_{m=0}^{n-1} A_{n,m}L_x^m + x\overline{P}^{(n)}(x)\right]. \qquad (12)$$

This expression holds for all four splitting functions, P^{gg}, P^{qg}, P^{gq} and P^{qq}. Explicit calculation of the leading P^{gg} coefficients gives, for example,

$$A_{1,0} = 6, \quad A_{2,1} = A_{3,2} = 0, \quad A_{4,3} = 518.4, \quad \ldots \qquad (13)$$

The general expansion (12) can be used to define various approximations:

- $(n = 1;\ m = 0) + \overline{P}^{(1)}$: LO GLAP.
- $(n = 1, 2;\ m = 0, 1) + \overline{P}^{(1,2)}$: NLO GLAP.
- $(n = 1;\ m = 0)$: 'double asymptotic scaling' (DAS).
- $(n \geq 1;\ m = n-1)$: leading-log in $1/x$ (LL_x).
- $(n \geq 1;\ m = n-1, n-2)$: next-to-leading-log in $1/x$ (NL_x).

Only the P^{gg} and P^{qg} splitting functions have non-zero LL_x coefficients in general. These leading contributions can be resummed using the BFKL equation [45] (see below), and eventually give rise to the characteristic

$$xg \sim x^{-\lambda}, \quad \lambda = \frac{12\ln 2\alpha_s}{\pi} \approx 0.5 \qquad (14)$$

BFKL behaviour at very small x. The NL_x contributions to P^{qg} and P^{qq} have recently been

calculated by Catani and Hautmann [37], while those for P^{gg} and P^{gq} remain unknown at present.

There are a number of important questions raised by the above observations. Clearly the fixed-order approximation to the evolution equation will break down when x is sufficiently small that $\alpha_s \ln(1/x) \sim 1$. Where and how does LO or NLO GLAP evolution break down, and can an 'improved' prediction be obtained by incorporating the resummed LL_x and NL_x contributions where these are known? A number of groups have recently performed numerical and analytical studies which attempt to answer these questions [38, 39, 40, 41] (see also [42, 43]). There appear to be at least two conclusions: (i) the importance of the higher-order $\ln(1/x)$ corrections is very dependent on the form of the starting distributions — steep starting distributions are evidently less affected than flat distributions; (ii) the dominant influence on the evolution of F_2 in the HERA kinematic region comes not from the leading P^{gg} or P^{gq} LL_x contributions, but rather from the formally subleading P^{qg} NL_x contribution. (Recall that $\partial F_2 \sim P^{qg} \otimes g$ at small x.)

There are however several important issues still to be clarified. At any order in perturbation theory, the full splitting functions satisfy momentum conservation sum rule constraints, for example

$$\int_0^1 dx\, x\, [P^{qg} + P^{gg}] = 0. \qquad (15)$$

This is *not* satisfied by the LL_x or NL_x contributions, and it is not clear to what extent momentum conservation is important for small-x evolution. Another issue concerns the factorisation scheme dependence at small x — changing schemes can move large L_x contributions from the splitting functions into the coefficient functions, see for example [43], and it may well be that the corrections to the evolution at small x are less important in some schemes than in others.

As an illustration of the above effects, we show in figure 11 (from Ref. [39]) the impact of the various approximations described above on the evolution of the F_2 structure function in the HERA kinematic regime. The input distributions at $Q_0^2 = 4$ GeV^2 are the 'flat' MRS(D_0') set [44]. The curves labelled '1-loop' and '2-loop' refer to LO and NLO GLAP evolution respectively. The 'L(x)' curve contains, in addition, the LL_x 'BFKL' contributions summed to all orders. As already stated, this has a very small impact on the evolution of F_2 in this kinematic range. The two curves labelled 'NLQ(x)' contain the resummed NL_x contributions to P^{qg} and P^{gq}. The difference between them is due to a different implementation of momentum conservation in each case, and may be taken as a very crude indication of the size of the unknown subleading contributions. It seems premature to draw any firm conclusions from figure 11,

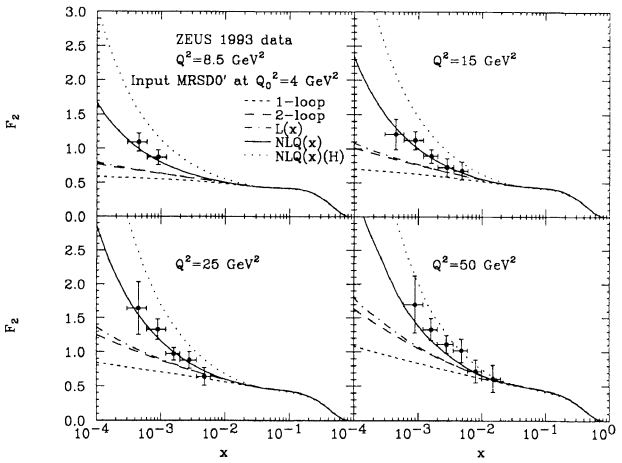

Figure 11. *Predictions for F_2^{ep} at HERA using various approximations for the splitting functions from Ref. [39], with data from ZEUS.*

except that large higher-order $\ln(1/x)$ contributions may indeed be important for HERA small-x structure functions, particularly if the starting distributions are flat.

3.2. Double Asymptotic Scaling

It is important to stress again that NLO GLAP evolution gives a perfectly good description of the HERA structure function data. In fact the data are consistent with a simple asymptotic approximation to the solution of the evolution equations known as 'double asymptotic scaling' [35, 36]. If at some Q_0^2 the small-x behaviour of the quark and gluon distributions $\sim x^{-\lambda}$ with $\lambda \lesssim 0$, then the behaviour in the *double asymptotic limit* $1/x, Q^2 \to \infty$ can be predicted from the LO (or NLO) GLAP equations. The key point is that the (LO) evolution is dominated by the $1/x$ part of the splitting functions, i.e. the $A_{1,0}$ coefficient in Eq. (12), and so the evolution equation (for the 'pure glue' theory) simplifies to

$$t\frac{\partial}{\partial t} g(x,t) \approx \frac{\alpha_s(t)}{2\pi} \frac{6}{x} \int_x^1 dy g(y,t), \qquad (16)$$

which can be solved analytically given suitable boundary conditions. Introducing the variables [36]

$$\sigma = \left[\ln(x_0/x) \ln\left(\ln(Q^2/\Lambda^2)/\ln(Q_0^2/\Lambda^2)\right)\right]^{1/2}$$
$$\rho = \left[\frac{\ln(x_0/x)}{\ln\left(\ln(Q^2/\Lambda^2)/\ln(Q_0^2/\Lambda^2)\right)}\right]^{1/2}, \qquad (17)$$

one finds the asymptotic solution

$$g(x,Q^2) \approx g(x_0,Q_0^2) \exp(2\gamma\sigma), \qquad (18)$$

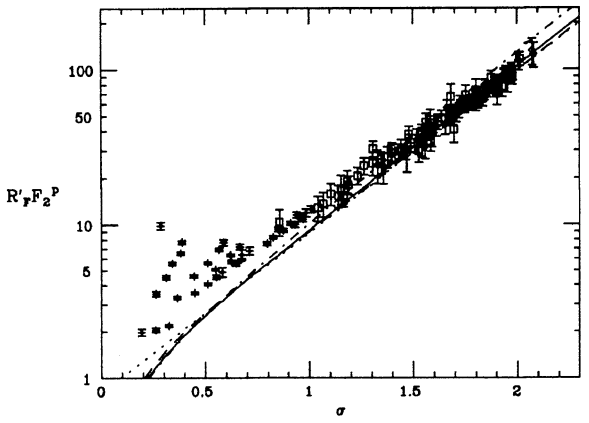

Figure 12. *$R'_F F_2$ as a function of σ, from Ref. [36]. The curves are described in the text, and the data are from NMC (crosses), H1 (squares) and ZEUS (diamonds).*

with $\gamma = [3/(\pi\beta_0)]^{1/2} = 6(33 - 2n_f)^{-1/2}$. Thus in the double asymptotic limit $1/x, Q^2 \to \infty$ the product $g\exp(-2\gamma\sigma)$ becomes independent of x and Q^2, equivalently ρ and σ.

Ball and Forte have generalised this result to the structure function F_2, including also the leading corrections, and made comparisons with the HERA data [36]. Their result is

$$F_2(x,Q^2) \approx A_0\sigma^{-1/2}\rho^{-1}\exp(2\gamma\sigma - \delta\sigma/\rho), \qquad (19)$$

with $A_0 = F_2(x_0, Q_0^2)$ and $\delta = 61/45$. Parameters x_0, Q_0 and Λ can be found such that the HERA F_2 data show clear evidence for the asymptotic scaling behaviour of Eq. (19). As an illustration, figure 12 [36] shows predictions and data for the quantity $R'_F F_2$, where

$$R'_F = \text{constant} \times \sigma^{1/2}\,\frac{\rho}{\gamma}\,\exp(\delta\sigma/\rho) \qquad (20)$$

as a function of σ for different values of ρ. The curves are obtained by evolving a typical soft gluon starting distribution and correspond to $\rho = 1.4$ (dot-dash), 2.2 (solid) and 3.2 (dashed). Also shown (dotted curve) is the best fit straight line (the predicted asymptotic behaviour) with slope $2\gamma = 12(33 - 2n_f)^{-1/2} = 2.4$ ($n_f = 4$). The parameters are $x_0 = 0.1$, $Q_0 = 1$ GeV, and $\Lambda = 263$ MeV. For large ρ and σ, the data and curves are consistent with a universal exponential increase ($\sim \exp(2\gamma\sigma)$), as predicted.

3.3. The BFKL description of F_2

Traditionally, simple parton model and Regge arguments were used to justify using gluon and sea quark 'starting distributions' which behave at small x as $x^{-\lambda}$ with $\lambda \approx 0$. In the previous sections we have seen how perturbative QCD evolution in Q^2 causes the distributions to rapidly develop a steeper shape. In the DAS limit the evolution equation sums leading powers of $[\alpha_s \ln(1/x)\ln(Q^2)]^n$ generated by multigluon emission, and the distributions increase faster than any power of $ln(1/x)$ as $x \to 0$. The dominant region of phase space is where the gluons have strongly-ordered transverse momenta, $Q^2 \gg k_{nT}^2 \gg \ldots \gg k_{1T}^2$. However such evolution does not include all the leading terms in the small-x limit. It neglects those terms which contain the leading power of $\ln(1/x)$ but which are not accompanied by the leading power of $\ln(Q^2)$. The BFKL equation [45], on the other hand, sums the leading $\ln(1/x)$ terms while retaining the full Q^2 dependence and not just the leading $\ln(Q^2)$ terms. The integration is taken over the full k_T phase space of the gluons, not just the strongly-ordered part. The result is most conveniently established for the gluon distribution unintegrated over k_T, and is (see the review by Martin [42] for further details),

$$f(x,k_T^2) \;\sim\; h(k_T^2)x^{-\lambda} \qquad (21)$$

where λ is the the maximum eigenvalue of the kernel of the BFKL equation

$$\frac{\partial f}{\partial L_x} = K \otimes f. \qquad (22)$$

For fixed α_s, $\lambda = 12\ln 2\alpha_s/\pi$ [45]. The prediction for F_2 is obtained by using the k_T-factorisation theorem [46]

$$F_2(x,Q^2) = \int_x^1 \frac{dx'}{x'}\int \frac{dk_T^2}{k_T^4} f\left(\frac{x}{x'},k_T^2\right)\overline{F}_2(x',k_T^2,Q^2) \qquad (23)$$

where $\overline{F}_2$ denotes the quark-box contribution $\gamma g \to q\bar{q}$ for the scattering of a photon of virtuality Q^2 off a gluon with longitudinal and transverse momenta x' and k_T respectively.

A complete numerical analysis of the solution of the BFKL equation and of the corresponding predictions for F_2, based on the above results, has been performed in Ref. [47]. The result can be summarised as

$$F_2(x,Q^2) = C(Q^2)x^{-\lambda} + F_2^{bkd}, \qquad (24)$$

where $\lambda \approx 0.5$ and F_2^{bkd} is a non-perturbative flat (at small x) background contribution. A very satisfactory description of the HERA data is obtained, see for example Ref. [42]. However the BFKL-based analysis is not entirely satisfactory: there are infra-red problems associated with integrating $\int dk_T^2 \alpha_s(k_T^2)$ down to $k_T^2 = 0$, which in practice means that the predictions depend to some extent on an undetermined infra-red cut-off parameter, and the next-to-leading (in L_x) corrections to the BFKL equation are as yet unknown.

There has been significant recent progress [48] towards a 'unified' treatment which incorporates both the GLAP and BFKL dynamics. An equation (the CCFM equation [49]) has been derived which reproduces the results of GLAP evolution at large x and BFKL behaviour at small x [50]. It will be interesting to see how the predictions of such an analysis compare in detail with the combined HERA and fixed-target data over the whole x range.

4. Structure functions at low Q^2

Interest in the form of deep inelastic structure functions at low Q^2 (by which we mean below a scale of a few GeV^2 which is generally taken as the boundary between the perturbative and non-perturbative regions) has been rekindled by data from the E665 collaboration [29]. In figure 13 these data are displayed together with data from the ZEUS collaboration at HERA. Note how the E665 data extends the HERA measurement range to lower Q^2 at the same (small) values of x. The combination of the two provides a large region of x and Q^2 values with which to test theoretical models. At higher x the same role is played by existing data from SLAC [14], which extend the x range typical of the BCDMS [34] and NMC [15] data sets to lower Q^2.

There have been various theoretical approaches to small-Q^2 structure functions. Various groups have constructed non-perturbative models based on Regge theory, Vector Meson Dominance models and the constraints of the photoproduction ($Q^2 \to 0$) limit, to extend low-Q^2 predictions to higher Q^2 [51, 52, 53, 54], either to interface with the Bjorken scaling of the parton model or the scaling violations of perturbative QCD.

For example, in the model of Ref. [54] the small-x F_2 structure function is taken to have the form

$$F_2(x,Q^2) = Ax^{-0.08}\frac{Q^2}{Q^2+a^2} + Bx^{0.45}\frac{Q^2}{Q^2+b^2}. \quad (25)$$

Here the powers of x are predicted by the power (Regge) behaviour of high-energy hadronic cross sections, and the requirement that $F_2 \sim Q^2$ as $Q^2 \to 0$ is implemented via form factors which also guarantee Bjorken scaling in the high-Q^2 limit. The parameters a^2 and b^2 are chosen to give good agreement with the measured structure functions. In particular, the E665 data are well-described, although the model cannot of course reproduce the scaling violations of perturbative QCD which are evident in the Q^2 dependence of the HERA data.

A second (perturbative-based) approach to describing low-Q^2 structure functions is to evolve the leading-twist GLAP-based high-Q^2 predictions *backwards* to lower Q^2. At some point this approach must fail: the coupling constant $\alpha_s(Q^2)$ will eventually become $\gg 1$,

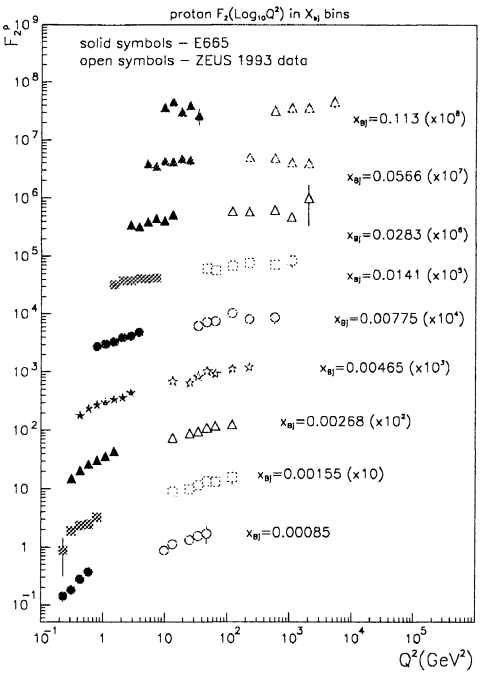

Figure 13. *The structure function $F_2^{\mu p} = F_2^{ep}$ from the E665 [29] and the ZEUS [22] collaborations.*

and higher-twist ($\mathcal{O}(1/Q^2)$) contributions to the structure functions will become equally important. However it is interesting to see how far down in Q^2 this approach can be made to work. In fact the GRV 'dynamical parton' distributions [9, 10] are based precisely on this approach. Leading-twist valence-like parton distributions are evolved upwards from a low starting scale (see Section 2.1 above). In the absence of any higher-twist contributions, the structure function is given simply by a charge-weighted sum over the quark distributions. This also gives a rather good description of the low-Q^2 E665 F_2 data, see Ref. [29], except for $Q^2 \lesssim 0.5\ GeV^2$ where the theoretical predictions fall rapidly to zero and undershoot the measurements. This signals a breakdown of the dynamical parton model description of structure functions at this scale.

The MRS group has also extended its global parton distribution analysis into the low-Q^2 region [5]. The aim is to provide a set of parton distributions that is consistent with the data taken at low Q^2 (down to $Q^2 \simeq 0.1\ GeV^2$) and, as Q^2 rises, smoothly approaches the set MRS(A) which is consistent with the high-Q^2 experimental data. This is achieved by modifying the

partons according to

$$q(x,Q^2) \rightarrow \frac{Q^2}{Q^2+m^2(x)} q(\xi,\hat{Q}^2), \qquad (26)$$

where

$$m^2(x) = Ax^{-n}, \quad \hat{Q}^2 = \max(Q^2, Q^2_{min}), \qquad (27)$$

and the target-mass variable is

$$\xi = \frac{2x}{1+r} \quad \text{with } r^2 = 1 + \frac{4M^2x^2}{Q^2}. \qquad (28)$$

The parameter $Q^2_{min} = 0.625\ GeV^2$ represents the lowest Q^2 value at which the backwards evolution of the standard MRS(A) set makes phenomenological sense. Below this, the distributions are 'frozen' in Q^2. At the same time, the distributions are modified by an overall form factor which has limits 0 and 1 at $Q^2 = 0, \infty$ respectively. The parameters A and n are fitted to data. Note that simple shadowing arguments do indeed suggest that the parameter $m^2(x)$ which appears in the form factor should increase as x decreases. Once again, a very good description of all the low Q^2 structure function data is obtained [5], and the model has a wider range of applicability in Q^2 than either the simple non-perturbative or dynamical parton approaches. An example of the description of the E665 structure function data at $x < 0.01$ is shown in figure 14.

In summary, various theoretical models have been used to successfully describe low-Q^2 structure function data. It seems, therefore, that a more rigorous theoretical approach is needed, to establish the validity of the various approximations and assumptions employed.

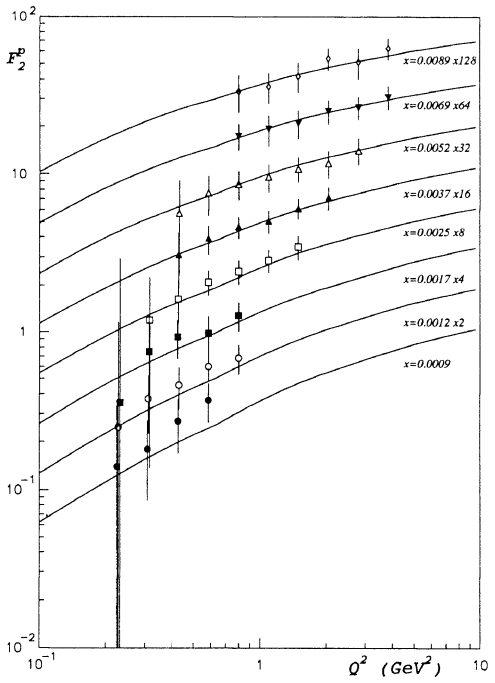

Figure 14. *The description of the E665 $F_2^{\mu p}$ [29] data for $x < 0.01$ by the MRS(A) modified parton distributions [5].*

5. Conclusions

The past year has seen several important advances in our understanding of the parton structure of hadrons. Over a large part of the x range the quark flavour structure is now very precisely known, to an accuracy of a few percent in the case of the u and d distributions. The gluon is, as always, less well determined, but a large quantity of data on large p_T jet, prompt photon, J/ψ, ... production remains to be exploited.

However most attention is at present focused on the small-x region. The theoretical framework of NLO GLAP gives an excellent description of the HERA F_2 data, either in the guise of (i) conventional parametrised input at $Q^2_0 = 4,\ 10,\ 20,\ \ldots\ \text{GeV}^2$, or (ii) (dynamical parton) valence-like input at $Q^2_0 \sim 0.3\ \text{GeV}^2$, or (iii) a flat, Regge-motivated input at $Q^2_0 \sim 1\ \text{GeV}^2$. The various versions of 'resummed $\ln(1/x)$' GLAP also appear to fit the data, but from different starting distributions since the higher-order effects are evidently large when such distributions are flat. Attempts to calculate the small-x structure functions from first principles, using for example the BFKL or CCFM formalisms, are also successful. One may hope that further, more precise measurements of the x and Q^2 dependence may discriminate between these scenarios. Alternatively, more definitive signatures may be found in less inclusive measures (energy flow, jet cross sections, ...) [55].

Finally, new low-Q^2 structure function data will be useful in bridging the gap between the perturbative and non-perturbative regimes, and in particular should allow more quantitative studies of higher-twist contributions.

Acknowledgements

It is a pleasure to thank the organizers for a most pleasant and stimulating meeting. Particular thanks go to Alan Martin and Dick Roberts for numerous enjoyable collaborations, the results of which form a large part of this review, and to those colleagues who have provided figures for inclusion in this presentation.

References

[1] G. Altarelli, N. Cabibbo, L. Maiani and R. Petronzio, Nucl. Phys. B69 (1974) 531.
M. Glück and E. Reya, Nucl. Phys. B130 (1977) 76.
[2] J.F. Owens, these proceedings.
[3] A. Vogt, these proceedings.
[4] A.D. Martin, R.G. Roberts and W.J. Stirling, Phys. Rev. D50 (1994) 6734.
[5] A.D. Martin, R.G. Roberts and W.J. Stirling, Phys. Rev. D51 (1995) 4756.
[6] A.D. Martin, R.G. Roberts and W.J. Stirling, Phys. Lett. B354 (1995) 155.
[7] CTEQ Collaboration (unpublished), see Ref. [8].
[8] CTEQ Collaboration: H.L. Lai et al., Phys. Rev. D51 (1995) 4763.
[9] M. Glück, E. Reya and A. Vogt, Z. Phys. C53 (1992) 127; Phys. Lett. B306 (1993) 391.
[10] M. Glück, E. Reya and A. Vogt, Z. Phys. C67 (1995) 433.
[11] L.N. Lipatov, Sov. J. Nucl. Phys. 20 (1975) 95.
V.N. Gribov and L.N. Lipatov, Sov. J. Nucl. Phys. 15 (1972) 438.
G. Altarelli and G. Parisi, Nucl. Phys. B126 (1977) 298.
Yu.L. Dokshitzer, Sov. Phys. JETP 46 (1977) 641.
[12] NA51 Collaboration: A. Baldit et al., Phys. Lett. B332 (1994) 244.
[13] CDF Collaboration: F. Abe et al., Phys. Rev. Lett. 74 (1995) 850.
[14] L.W. Whitlow et al., Phys. Lett. B282 (1992) 475.
[15] NMC Collaboration: P. Amaudruz et al., Phys. Lett. B295 (1992) 159.
[16] CCFR Collaboration: P.Z. Quintas et al., Phys. Rev. Lett. 71 (1993) 1307.
[17] A.D. Martin, R.G. Roberts and W.J. Stirling, Phys. Lett. B308 (1993) 377.
[18] CCFR Collaboration: A.O. Bazarko et al., Z. Phys. C65 (1995) 189.
[19] A. Capella, A. Kaidalov, C. Merino and J. Tran Thanh Van, Phys. Lett. B337 (1994) 358.
[20] C. Bourrely and J. Soffer, Nucl. Phys. B445 (1995); Phys. Rev. D51 (1995) 2108.
[21] H1 Collaboration: J. Dainton, these proceedings.
[22] ZEUS Collaboration: B. Foster, these proceedings.
[23] J. Huston, E. Kovacs, S. Kuhlmann, H.L. Lai, J.F. Owens and W.-K. Tung, Phys. Rev. D51 (1995) 6139.
[24] M. Glück, L.E. Gordon, E. Reya and W. Vogelsang, Phys. Rev. Lett. 73 (1994) 388.
[25] A. Vogt and W. Vogelsang, preprint DESY-95-096 (1995) and Ref. [3].
[26] CDF collaboration: F. Abe et al., Phys. Rev. Lett. 73 (1994) 2662.
[27] UA2 collaboration: J. Alitti et al., Phys. Lett. B299 (1993) 174.
[28] A. Milsztajn and M. Virchaux, Phys. Lett. B274 (1992) 221.
[29] H. Schellman, these proceedings.
[30] P. Renton, private communication.
[31] A.D. Martin, R.G. Roberts and W.J. Stirling, Phys. Rev. D43 (1991) 3648.
[32] A. Vogt, Phys. Lett. B354 (1995) 145.
[33] A.D. Martin, R.G. Roberts and W.J. Stirling, Phys. Lett. B356 (1995) 89.
[34] BCDMS Collaboration: A.C. Benvenuti et al., Phys. Lett. B223 (1989) 485.
[35] A. De Rujula, S.L. Glashow, H.D. Politzer, S.B. Treiman, F. Wilczek and A. Zee, Phys. Rev. D10 (1974) 1649.
[36] R.D. Ball and S. Forte, Phys. Lett. B335 (1994) 77 and B336 (1994) 77.
[37] S. Catani and F. Hautmann, Nucl. Phys. B427 (1994) 475.
[38] R.K. Ellis, E. Levin and Z. Kunszt, Nucl. Phys. B420 (1994) 517; erratum B433 (1995) 498.
[39] R.K. Ellis, F. Hautmann and B.R. Webber, Phys. Lett. B348 (1995) 582.
[40] R.D. Ball and S. Forte, Phys. Lett. B351 (1995) 513.
[41] J.R. Forshaw, R.G. Roberts and R.S. Thorne, Phys. Lett. B356 (1995) 79.
[42] A.D. Martin, these proceedings.
[43] S. Catani, these proceedings.
[44] A.D. Martin, R.G. Roberts and W.J. Stirling, Phys. Lett. B306 (1993) 145.
[45] E.A. Kuraev, L.N. Lipatov and V.S. Fadin, Phys. Lett. B60 (1975) 50; Sov. Phys. JETP 44 (1976) 433 and 45 (1977) 199.
Ya.Ya. Balitsky and L.N. Lipatov, Sov. J. Nucl. Phys. 28 (1978) 822.
[46] S. Catani, M. Ciafaloni and F. Hautmann, Phys. Lett. B242 (1990) 97; Nucl. Phys. B366 (1991) 657.
[47] A.J. Askew, J. Kwiecinski, A.D. Martin and P.J. Sutton, Phys. Rev. D47 (1993) 3775 and D49 (1994) 4402.
[48] G. Marchesini, these proceedings.
[49] M. Ciafaloni, Nucl. Phys. B296 (1988) 49.
S. Catani, F. Fiorani and G. Marchesini, Phys. Lett. B234 (1990) 339; Nucl. Phys. B336 (1990) 18.
[50] J. Kwiecinski, A.D. Martin and P.J. Sutton, Phys. Rev. D52 (1995).
[51] B. Badelek and J. Kwiecinski, Zeit. Phys. C43 (1989) 251; Phys. Lett. B295 (1992) 263.
[52] H. Abramowicz, E.M. Levin, A. Levy and U. Maor, Phys. Lett. B269 (1991) 465.
[53] NMC Collaboration: P. Amaudruz et al., Nucl. Phys. B273 (1992) 3.
[54] A. Donnachie and P.V. Landshoff, Zeit. Phys. C61 (1994) 139.
[55] B.R. Webber, these proceedings.